THE PUBLISHING HOUSE
OF THE ROMANIAN ACADEMY

PROCEEDINGS OF THE ROMANIAN ACADEMY, Series A,
Volume 23, Number 3/2022, pp. 279–288

KINEMATICS AND WORKSPACE ANALYSIS OF AN INNOVATIVE 6-DOF PARALLEL ROBOT FOR SILS

Doina PISLA, Iosif BIRLESCU, Alexandru PUSCA, Paul TUCAN, Bogdan GHERMAN,
Adrian PISLA, Tiberiu ANTAL, Calin VAIDA

Technical University of Cluj-Napoca, Research Center for Industrial Robots Simulation and Testing, Romania
Corresponding author: Iosif BIRLESCU, E-mail: iosif.birlescu@mep.utcluj.ro

Abstract. The paper presents the kinematic and workspace analysis of a 6-DOF parallel robot for Single Incision Laparoscopic Surgery (SILS), a type of minimally invasive surgery where the surgical instruments are inserted into the operating field through a single port (trocar). First, the robotic-assisted task is defined (as a medical protocol) and then the kinematic models of the parallel robot are obtained using a vector method. While an analytical solution is derived for the parallel robot inverse kinematics, its forward kinematics is numerically solved. The workspace generation and the initial numerical simulations, performed with respect to the required medical task, validate the robotic system for the SILS medical task.

***Keywords**:* parallel robot, kinematics, workspace, robotic-assisted surgery, SILS.

1. INTRODUCTION

Single incision laparoscopic surgery (SILS) is a type of minimal invasive surgery (MIS) which uses a single access port for the surgical instruments' insertion (using a specialized elastic trocar) within the operating field (in contrast to classical MIS where the instruments are inserted through distinct access ports). The most significant advantages of SILS over classical MIS and open surgery are: (i) less surgical trauma and pain for the patients; (ii) faster patient recovery (i.e., less hospital time); (iii) better cosmetics [1]. However, using a single access port leads to major challenges for SILS, mainly due to the small volume for the surgical instruments' manipulation (especially outside the operating field where the "crossing" phenomenon usually occurs and the surgeon guides the distal tip of the right instrument with its left hand and vice-versa), which in turn negatively affects the procedure ergonomics. Both drawbacks may affect patient safety [2]. As history showed, robotic assisted surgery revolutionized the field, e.g., in the year 2000 the da Vinci robot entered the healthcare domain with great success in MIS, and later in 2018 the same company developed the da Vinci SP robotic system, a platform that targets SILS exclusively [3]. Robotic-assisted MIS (including SILS) has distinct advantages over the hand performed procedure. The master-slave robotic systems offer increased accuracy, scalable motions, better ergonomics, among others [4, 5]. The benefits of the robotic assisted procedure directly translate in: less postoperative pain, reduces scarring, less length of hospital stay, short recovery time. Several robotic systems designed for SILS are described in the literature. The da Vinci SP system [6] uses a single highly dexterous instrument positioned by a single robotic arm at the SILS access port. The SP instrument "unfolds" and provides three active instruments and a endoscopic camera (all of them being flexible). Senhance [7] is another FDA approved robotic system. In contrast to the da Vinci SP platform, Senhance uses a multi-arm approach which may cause collision issues (among the robot arms). A different approach was studied in [4], where the authors proposed a hybrid robotic system consisting of a serial robot that positions a parallel orientation platform near the SILS access port, which in turn guides the active surgical instruments. In [8] the authors show a robotic system that is able to position a laparoscopic camera, or an active surgical instrument in the operating field (which could be used in SILS).

Parallel robots are a good option to be used for a SILS robotic assisted procedure since they have excellent accuracy, repeatability and they can work properly in narrow operating field (required in SILS). A specialized orientation platform that guides the active instruments can be mounted on the mobile platform to achieve the necessary motions for the surgical instruments. This new approach avoids some of the shortcomings of multi-arm systems (i.e., robotic arm collisions) and of purely dexterous instruments (which in some configurations may lose gripping force, negatively affecting e.g., suturing). The paper introduces an innovative parallel robotic system for SILS and presents its kinematic modeling, and numerical results for the robot trajectory generation correlated with the SILS task. The motivation is to prove the viability of the robotic system for the medical task and establish the theoretical basis for future development.

The paper is structured as follows: Section 2 introduces the parallel robot and describes the robotic-assisted medical task; Section 3 presents the parallel robot kinematic models, starting from the geometric ones and ending with the velocity and acceleration ones. Section 4 shows numerical results for trajectory planning with respect to the SILS task. Section 5 presents the paper conclusions.

2. A NEW PARALLEL ROBOT FOR SILS

A simplified CAD model of the new parallel robotic system for SILS is presented in Fig. 1 (patent pending [9]). The robotic system consists of three major components: i) a 6-DOF parallel robot (Fig. 1b) which is positioned on the side of the operating table (Fig. 1a), which guides a mobile platform; ii) the mobile platform contains a laparoscopic camera and two additional orientation platforms with 3-DOF each, positioned on both sides of the laparoscope, for the active instrument manipulation (Fig. 1c); iii) two active SILS instruments (with 4-DOF [4]) are guided by the orientation platforms using RCM [10]. The robotic system has multiple redundant DOF to ensure good accuracy for the tissue manipulation in the operating field. Furthermore, the SILS robotic system will contain AI and VR modules [14] to help the surgeons both in the preplanning stage (e.g., to visualize the operating field), and during the procedure (e.g., AI with suggestive behaviour that highlight bleeding).

A preliminary robotic-assisted protocol was developed in cooperation with medical specialists for the new SISL robot; the protocol uses a sequential approach to ensure patient safety. Table 1 presents this protocol for a clear understanding of the robot task and its intended operation.

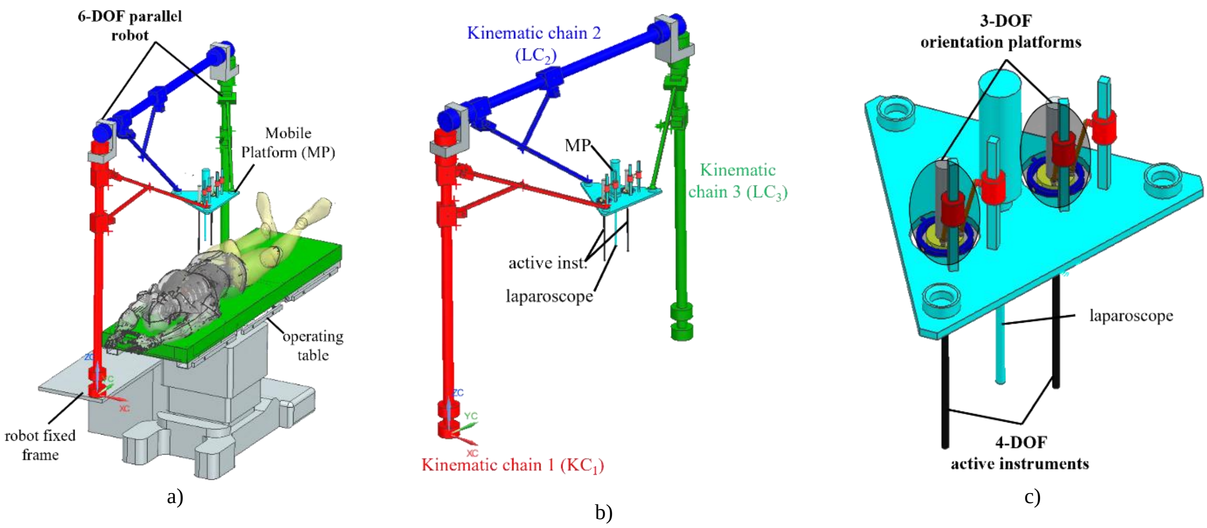

Fig 1 – CAD model of the new SILS parallel robotic system: a) parallel robotic system positioned near the operating table; b) 6-DOF parallel robot; c) mobile platform containing two 3-DOF orientation platforms for guiding the active instruments.

Table 1

Robotic-assisted SILS protocol

Procedure's steps	Detail
Step 1 Preplanning	**1.1** medical history analysis and diagnosis; **1.2** defining the therapeutic conduit using the SILS robotic system AI and VR tools with embedded medical imaging and other medical parameters; **1.3** defining the robot-patient relative position and estimating the RCM point (corrections may be done in situ); **1.4** estimate the optimum mobile platform position and orientation to ensure adequate workspace in the operating field using the VR modules of the SILS robotic system; **1.5** performing a simulated procedure using the SILS robotic system AI and VR modules.
Step 2 Preparation	**2.1** preparing the patient and the robotic system; **2.2** mounting the (sterile) SILS instruments and the laparoscope; **2.3** testing the robotic system to ensure proper functionality (performed by the main surgeon from the master console, with the assistant surgeon analysing output motions for the surgical instruments); **2.4** preparing the operating field (anaesthesia, incision, SILS trocar insertion, CO_2 insufflation).
Step 3 Go to Ins. point	**3.1** moving the parallel robot mobile platform towards the insertion point (all the instruments should be aligned with the SILS trocar and have a vertical pose checked by the AI modules and confirmed by the assistant surgeon); **3.2** visual confirmation for the instruments position with respect to the SILS trocar (assistant surgeon); **3.3** manually position the SILS instruments in their access ports (assistant surgeon).
Step 4 Instr. insertion	**4.1** the parallel robotic system inserts all the SILS instruments in the operating filed by guiding the mobile platform on a linear vertical direction; **4.2** continuous visual confirmation for the instrument insertion (minor corrections can be done manually by the assistant surgeon).
Step 5 Mobile platform positioning	**5.1** the parallel robotic system positions and orients the mobile platform (predefined in Step 1 using the VR and AI modules) using RCM; **5.2** positioning and orientation corrections can be applied, if necessary, from the master console; **5.3** visual confirmation for the instruments, trocar, external tissue (assistant surgeon).
Step 6 Surgical task	**6.1** locking the robot platform and operating the SISL active instruments; **6.2** mobile platform repositioning may be performed (using RCM), if required, for better view through the laparoscope or instrument handling (*Important:* if this step is required the robot must compensate the active instrument tip position such as the relative position between the tissue and the tissue is unchanged); **6.3** performing the SILS task (the VR and AI agents help the surgeon in to ensure patient safety and ergonomics).
Step 7 Instr. retraction	**7.1** manipulating the active instruments (through the orientation platform and their self DOF) to enable adequate retraction on a linear path; **7.2** instrument retraction using a linear path; 7.3 continuous visual confirmation, both outside the operating field (assisting surgeon) and inside using the laparoscope (main surgeon); **7.3** manual assistance if required.
Step 8 Robot homing	**8.1** sending the robot to the safe position;
Step 9 Procedure finalizing	**9.1** removal of CO_2 from the patient's body; **9.2** trocar extraction; **9.3** tissue suture and ensuring homeostasis.

3. KINEMATIC MODELING

The mathematical modelling from this point onward is focused exclusively on the 6-DOF parallel robot. Other studies reported kinematic analysis of the orientation platform [11] or the active SILS instruments [5]. The kinematic scheme of the 6-DOF parallel robot is presented in Fig. 2 showing a parallel mechanism of type 3-R-PRR-PRS, which consists of three identical kinematic chains and a mobile platform with the topology:

- The three identical kinematic chains LC_1, LC_2, and LC_3 (type R-PRR-PRS) are actuated by the prismatic joints q_1, q_2 (for LC_1), q_3, q_4 (for LC_2), and q_5, q_6 (for LC_3), respectively. Each chain has a passive rotation motion around the actuation axis of their respective prismatic joints. Furthermore, each chain contains other three passive revolute joints namely: R_{11}, R_{12}, R_{13} for LC_1, R_{21}, R_{22}, R_{23} for LC_2, R_{31}, R_{32}, R_{33} for LC_3. Lastly, each kinematic chain contains a passive spherical joint (S_1, S_2, and S_3, respectively) that connect the chain with the mobile platform. The geometric parameters of the kinematic chains are: l_0 is the distance between the actuation axes of the joint pairs q_1, q_2 (l_0 in a horizontal plane), q_3, q_4 (l_0 in a vertical plane), and q_5, q_6 (l_0 in a horizontal plane), respectively; l_1 and l_2 represent the mechanical links that (together with the passive revolute joints) compose the kinematic chains; L_H represents the distance between the actuation axis of LC_1 and LC_3 (on OY direction); L_V represents the distance between axis OY and the actuation axis of LC_2;

- The mobile platform (*MP*) is connected to the three kinematic chains through the three passive spherical joints S_1, S_2 and S_3. The geometric parameter l_p represents the side of the equilateral triangle defining the *MP* with vertices the centres of the passive joints S_1, S_2 and S_3;
- Two coordinate systems are defined, the fixed one *OXYZ* attached to the robot base such that the actuation axis of q_1 and q_2 represents the *OZ* axis, and the mobile one *O'X'Y'Z'* attached to the geometric centre of the *MP* (Fig. 2).

For the **mechanism synthesis** the formula presented in [12] is used, which defines:

$$M = (6-F)\cdot N - \sum_{i=1..5}(i-F)\cdot C_i \tag{1}$$

where: M represents the mobility degree of the mechanism; F represents the mechanism family (the number of common constraints among the mobile elements); N the mobile elements within the mechanism; C_i the class i joints (i – the number of suppressed degrees of freedom of a mechanical joint). Considering that each input kinematic chain represents a class 3 joint, and each kinematic chain and the mobile platform are mobile elements results in: $F = 0$ (MP has no constraints), $N = 4$, and $C_3 = 6$. Substituting these values in Eq. (1) shows that the SILS parallel robot has 6-DOF:

$$M = 6\cdot N - 3\cdot C_3 = 6. \tag{2}$$

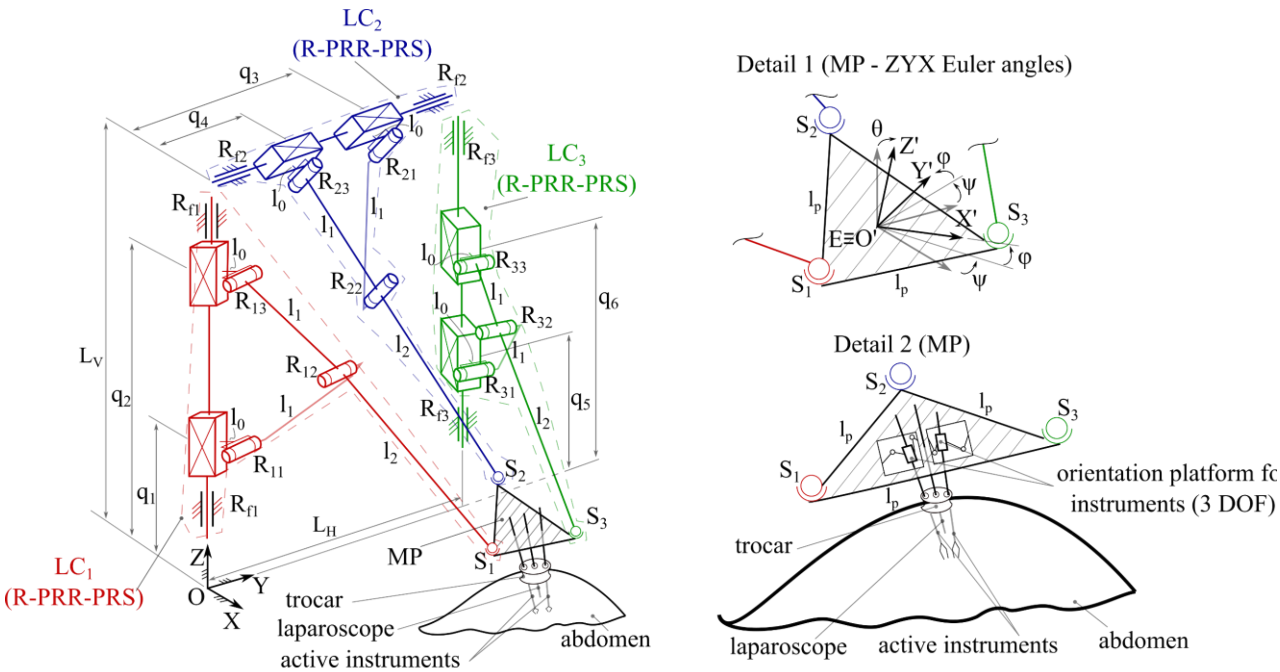

Fig. 2 – The kinematic of the parallel robotic system (type 3-R-PRR-PRS) for SILS.

3.1. Geometric modeling

For the **inverse geometric model**, the inputs are defined by the vector $X = [X_E, Y_E, Z_E, \psi, \theta, \varphi]^T$ (the coordinates and orientations of the mobile platform) whereas the outputs are the generalized coordinates of the active joints defined by $Q = [q_1, q_2, q_3, q_4, q_5, q_6]^T$. The *ZYX* Euler angle convention is used with the rotation matrices:

$$R_Z(\psi) = \begin{bmatrix} c_\psi & -s_\psi & 0 \\ s_\psi & c_\psi & 0 \\ 0 & 0 & 1 \end{bmatrix}, \quad R_Y(\theta) = \begin{bmatrix} c_\theta & 0 & s_\theta \\ 0 & 1 & 0 \\ -s_\theta & 0 & c_\theta \end{bmatrix}, \quad R_X(\varphi) = \begin{bmatrix} 1 & 0 & 0 \\ 0 & c_\varphi & s_\varphi \\ 0 & -s_\varphi & c_\varphi \end{bmatrix}, \tag{3}$$

where $c_\psi = \cos(\psi)$, $s_\psi = \sin(\psi)$, $c_\theta = \cos(\theta)$, $s_\theta = \sin(\theta)$, $c_\varphi = \cos(\varphi)$, $s_\varphi = \sin(\varphi)$. The Euler transformation matrix, denoted M, is obtained by multiplying the rotation matrices:

$$M = R_Z(\psi)\cdot R_Y(\theta)\cdot R_X(\varphi). \tag{4}$$

The coordinates of the centers of the spherical joints (S_1, S_2, S_3) with respect to the mobile coordinate frame:

$$S'_1:\begin{cases} X'_{S1} = \dfrac{\sqrt{3}}{6}l_p \\ Y'_{S1} = -\dfrac{1}{2}l_p \\ Z'_{S1} = 0 \end{cases},\quad S'_2:\begin{cases} X'_{S2} = -\dfrac{\sqrt{3}}{3}l_p \\ Y'_{S2} = 0 \\ Z'_{S3} = 0 \end{cases},\quad S'_3:\begin{cases} X'_{S3} = \dfrac{\sqrt{3}}{6}l_p \\ Y'_{S3} = \dfrac{1}{2}l_p \\ Z'_{S3} = 0 \end{cases} \tag{5}$$

Using the vector relations:

$$S_i:[X_{Si},Y_{Si},Z_{Si}]^{\mathrm{T}} = [X_E,Y_E,Z_E]^{\mathrm{T}} + M\cdot[X'_{Si},Y'_{Si},Z'_{Si}]^{\mathrm{T}},\;\; i=1...3, \tag{6}$$

yields the coordinates of the passive spherical joints (S_1, S_2, S_3) with respect to the fixed coordinate frame *OXYZ*:

$$S_1:\begin{cases} X_{S1} = X_E + \dfrac{\sqrt{3}}{6}l_p\,c_\psi\,c_\theta - \dfrac{1}{2}l_p\,c_\psi\,s_\theta\,s_\varphi + \dfrac{1}{2}l_p\,s_\psi\,c_\theta \\ Y_{S1} = Y_E + \dfrac{\sqrt{3}}{6}l_p\,s_\psi\,c_\theta - \dfrac{1}{2}l_p\,s_\psi\,s_\theta\,s_\varphi - \dfrac{1}{2}l_p\,c_\psi\,c_\theta \\ Z_{S1} = Z_E - \dfrac{\sqrt{3}}{6}l_p\,s_\theta - \dfrac{1}{2}l_p\,s_\varphi\,c_\theta \end{cases},\quad S_2:\begin{cases} X_{S2} = X_E - \dfrac{\sqrt{3}}{3}l_p\,c_\psi\,c_\theta \\ Y_{S2} = Y_E - \dfrac{\sqrt{3}}{3}l_p\,s_\psi\,c_\theta \\ Z_{S2} = Z_E + \dfrac{\sqrt{3}}{3}l_p\,s_\theta \end{cases},$$

$$S_3:\begin{cases} X_{S3} = X_E + \dfrac{\sqrt{3}}{6}l_p c_\psi c_\theta + \dfrac{1}{2}l_p c_\psi s_\theta s_\varphi - \dfrac{1}{2}l_p s_\psi c_\theta \\ Y_{S3} = Y_E + \dfrac{\sqrt{3}}{6}l_p s_\psi c_\theta + \dfrac{1}{2}l_p s_\psi s_\theta s_\varphi + \dfrac{1}{2}l_p c_\psi c_\theta \\ Z_{S3} = Z_E - \dfrac{\sqrt{3}}{6}l_p s_\theta + \dfrac{1}{2}l_p s_\varphi c_\theta \end{cases} \tag{7}$$

Based on the kinematic scheme (Fig. 2) the distances R_i (i =1…3) between the passive spherical joints and the actuation axes of q_i (i =1…6) can be computed using trigonometry:

$$R_{1,2,3} = \frac{1}{2l_1}\left(l_1 + l_2\right)\sqrt{4l_1^2 - \left(q_{2,4,6} - q_{1,3,5}\right)^2} + l_0 \tag{8}$$

$$X_{S1}^2 + Y_{S1}^2 - R_1^2 = 0\,,\; X_{S2}^2 + \left(Z_{S2} - L_V\right)^2 - R_2^2 = 0\,,\; X_{S3}^2 + \left(Y_{S3} - L_H\right)^2 - R_3^2 = 0. \tag{9}$$

The circle equations (Eq. (9)) are solved for q_i (i =1…6) yielding double solutions for the active joints. To describe the intended working mode of the parallel robot (the one illustrated in Fig. 2) the following constraints are imposed (to establish limits for the actuation axes such that specific singularities are avoided when e.g., $q_1 = q_2$): $q_1 < q_2$, $q_3 > q_4$, $q_5 < q_6$ and the explicit closed form solutions for the inverse geometric model are:

$$\begin{cases} q_1 = \dfrac{1}{l_1+l_2}\left[(l_1+l_2)q_2 - 2l_1\sqrt{-X_{S1}^2 - Y_{S1}^2 - l_0^2 + (l_1+l_2)^2 + 2l_0\sqrt{X_{S1}^2+Y_{S1}^2}}\right] \\ q_2 = \sqrt{(l_1+l_2)^2 - X_{S1}^2 - Y_{S1}^2 - l_0^2} + Z_{S1} \\ q_3 = \dfrac{1}{l_1+l_2}\left[(l_1+l_2)q_4 + 2l_1\sqrt{-X_{S2}^2 - l_0^2 + (l_1+l_2)^2 - (L_V - Z_{S2})^2 + 2l_0\sqrt{(L_V - Z_{S2})^2 + X_{S2}^2}}\right] \\ q_4 = Y_{S2} - \sqrt{(l_1+l_2)^2 - X_{S2}^2 - l_0^2 - (L_V - Z_{S2})^2} \\ q_5 = \dfrac{1}{l_1+l_2}\left[(l_1+l_2)q_6 - 2l_1\sqrt{-X_{S3}^2 - l_0^2 + (l_1+l_2)^2 - (L_H - Y_{S3})^2 + 2l_0\sqrt{(L_H - Y_{S3})^2 + X_{S3}^2}}\right] \\ q_6 = \sqrt{(l_1+l_2)^2 - X_{S3}^2 - (L_H - Y_{S3})^2 - l_0^2} + Z_{S3} \end{cases} \tag{10}$$

For the **forward geometric model**, the inputs are the active joints coordinates $Q = [q_1, q_2, q_3, q_4, q_5, q_6]^T$, whereas the outputs are $X = [X_E, Y_E, Z_E, \psi, \theta, \varphi]^T$. The input-output equations for the mathematical model are obtained by using Eqs. (7)–(9), defining 6 nonlinear equations with the outputs $X_E, Y_E, Z_E, \psi, \theta, \varphi$ as unknowns:

$$\begin{cases} f_1 : \dfrac{1}{6l_1}\left[l_p l_1\left(\sqrt{3}\mathrm{s}_\theta + 3\mathrm{c}_\theta \mathrm{s}_\varphi\right) + 3(q_1 + q_2 - 2Z_E) + 3l_2(q_1 - q_2)\right] = 0 \\ f_2 : \dfrac{1}{12l_1}\Bigg[-12l_0 l_1(l_1+l_2)\sqrt{4l_1^2 - (q_1-q_2)^2} + 4\sqrt{3}l_1 l_p\left(X_E\mathrm{c}_\psi + Y_E\mathrm{s}_\psi - \dfrac{1}{2}l_p\mathrm{s}_\varphi\mathrm{s}_\theta\right)\mathrm{c}_\theta + l_1 l_p^2\left(3\mathrm{c}_\varphi^2 - 2\right)\mathrm{c}_\theta^2 - \\ \quad -12l_1 l_p\left(\left(X_E\mathrm{c}_\psi + Y_E\mathrm{s}_\psi\right)\mathrm{s}_\varphi\mathrm{s}_\theta - \left(X_E\mathrm{s}_\psi - Y_E\mathrm{c}_\psi\right)\mathrm{c}_\varphi\right) - 12l_1^2(l_1 + 2l_2) + 12l_1\left(X_E^2 + Y_E^2 - l_0^2 - l_2^2\right) + \\ \quad + 3l_1\left(l_p^2 - (q_1+q_2)^2\right) + 6l_2(q_1-q_2)^2 + 3\dfrac{l_2^2}{l_1}(q_1-q_2)^2\Bigg] = 0 \\ f_3 : \dfrac{1}{6l_1}\left[2\sqrt{3}l_p l_1\mathrm{s}_\psi\mathrm{c}_\theta + 3(q_3 + q_4 - 2Y_E) + 3l_2(q_3 - q_4)\right] = 0 \\ f_4 : \dfrac{1}{12l_1}\Bigg[-12l_0 l_1(l_1+l_2)\sqrt{4l_1^2 - (q_3-q_4)^2} - 8\sqrt{3}l_1 l_p\left(X_E\mathrm{c}_\psi\mathrm{c}_\theta + (L_V - Z_E)\mathrm{s}_\theta\right) + 4l_1 l_p^2\left(3\mathrm{c}_\psi^2 - 1\right)\mathrm{c}_\theta^2 - \\ \quad -12l_1^2(l_1+2l_2) + 12l_1\left((L_V - Z_E)^2 + X_E^2 - l_0^2 - l_2^2\right) + l_1\left(4l_p^2 - 3(q_3-q_4)^2\right) \\ \quad + 3\left(2l_2 + \dfrac{l_2^2}{l_1}\right)(q_3-q_4)^2\Bigg] = 0 \\ f_5 : \dfrac{1}{6l_1}\left[l_p l_1\left(\sqrt{3}\mathrm{s}_\theta - 3\mathrm{s}_\varphi\mathrm{c}_\theta\right) + 3(q_5 + q_6 - 2Z_E) + 3l_2(q_5 - q_6)\right] = 0 \\ f_6 : \dfrac{1}{12l_1}\Bigg[-12l_0 l_1(l_1+l_2)\sqrt{4l_1^2 - (q_5-q_6)^2} - 4\sqrt{3}l_1 l_p\left((L_H - Y_E)\mathrm{s}_\psi - \dfrac{1}{2}l_p\mathrm{s}_\varphi\mathrm{s}_\theta - X_E c_\psi\right)\mathrm{c}_\theta + \\ \quad + l_1 l_p^2\left(3\mathrm{c}_\varphi^2 - 2\right)\mathrm{c}_\theta^2 - 12l_1 l_p\left((L_H - Y_E)\mathrm{s}_\varphi\mathrm{s}_\theta + X_E\mathrm{c}_\varphi\right) + 12l_1 l_p\left(X_E\mathrm{s}_\varphi\mathrm{c}_\psi\mathrm{s}_\theta - (L_H - Y_E)\mathrm{c}_\psi\mathrm{c}_\theta\right) - \\ \quad -12l_1^2(l_1+2l_2) + 12l_1\left((L_H - Y_E)^2 + X_E^2 - l_0^2 - l_2^2\right) + 3l_1\left(l_p^2 + (q_5-q_6)^2\right) + 3\left(2l_2 + \dfrac{l_2^2}{l_1}\right)(q_5-q_6)^2\Bigg] = 0. \end{cases} \tag{11}$$

Equation (11) can be solved numerically using the Newton-Raphson (NR) algorithm. To apply NR the geometric parameters of the parallel robot are given, as well as the inputs $Q = [q_1, q_2, q_3, q_4, q_5, q_6]^T$ and an initial solution (guess) for the outputs $Sol_0 = [X_{E\_0}, Y_{E\_0}, Z_{E\_0}, \psi_0, \theta_0, \varphi_0]$ (computed via the inverse geometric model from a previous neighboring point on the robot trajectory). The Jacobian matrix A is computed by differentiating f_i (i =1…6) from Eq. (11) with respect to the outputs $X = [X_E, Y_E, Z_E, \psi, \theta, \varphi]$, and the following relations are iteratively applied:

$$\mathrm{Sol}_i = \mathrm{Sol}_{i-1} + \Delta_i, \quad \Delta_i = -A^{-1}_{num\_i} \cdot F_{num\_i}, \quad i = 1...n, \tag{12}$$

where Sol_i – the solution (for $X_E, Y_E, Z_E, \psi, \theta, \varphi$) after the i^{th} iteration, A_{num_i} – the Jacobian matrix A evaluated with the geometric parameters and Sol_{i-1}, F_{num_i} – the input-output equations (Eq. (11)) evaluated with Sol_{i-1}.

3.2. Kinematic modeling

To compute the **velocity kinematics** the Jacobian matrix formulation is used [13]:

$$A \cdot \dot{X} + B \cdot \dot{Q} = 0 \tag{13}$$

were A represents the Jacobian matrix computed by differentiating the implicit functions f_i (i=1…6) (Eq. 11), with respect to $[X_E, Y_E, Z_E, \psi, \theta, \varphi]$, B represents the Jacobian matrix computed by differentiating f_i (i =1…6), with respect to $[q_1, q_2, q_3, q_4, q_5, q_6]$, $\dot{X}$ represents velocity vector of the mobile platform, and $\dot{Q}$ represents the velocity vector of the active joints [15]. Using Eq. (13) the explicit solutions for the velocity kinematics are:

$$\dot{Q} = -B^{-1} \cdot A \cdot \dot{X} \tag{14}$$

$$\dot{X} = -A^{-1} \cdot B \cdot \dot{Q}, \tag{15}$$

where Eq. (14) represents the solution for the inverse kinematic model (for velocities) and Eq. (15) represents the solution for the forward geometric model (for velocities).

To compute the acceleration kinematics Eq. (13) is differentiated with respect to time yielding:

$$\dot{A} \cdot \dot{X} + A \cdot \ddot{X} + \dot{B} \cdot \dot{Q} + B \cdot \ddot{Q} = 0, \tag{16}$$

where $\dot{A}$ and $\dot{B}$ are the time derivative of the Jacobian matrices, $\ddot{X}$ and $\ddot{Q}$ are the acceleration vectors for the mobile platform (coordinates and orientations) and the active joints respectively. To solve the kinematic models Eq. (16) can be rewritten as:

$$\ddot{Q} = -B^{-1} \cdot \left(\dot{A} \cdot \dot{X} + A \cdot \ddot{X} + \dot{B} \cdot \dot{Q} \right) \tag{17}$$

$$\ddot{X} = -A^{-1} \cdot \left(\dot{A} \cdot \dot{X} + \dot{B} \cdot \dot{Q} + B \cdot \ddot{Q} \right) \tag{18}$$

where Eq. (17) represents the solution for the inverse kinematics (for accelerations), whereas Eq. (18) represents the solution for the forward kinematics (for accelerations).

4. NUMERICAL RESULTS

The workspace for the 6-DOF parallel robot was computed using the robot inverse geometric model by defining discrete volumes and computing the active joints values q_i (i =1…6) for each point form the defined volumes. If the solution was real and the active joints did not exceed the axis limits $q_1 < q_2 < L_V$, $q_4 < q_3 < L_H$, $q_5 < q_6 < L_V$ the point was saved, otherwise the point was discarded. The following numerical values for the 6-DOF parallel robot geometric parameters were used $\{l_0 = 75, l_1 = 300, l_2 = 400, l_p = 300, L_H = 1500, L_V = 1550\}$ [mm]. Fig. 3.a shows the workspace of the parallel robot computed for the mobile platform with no orientation ($\psi = \theta = \varphi = 0°$) (constraint used when the mobile platform is aligned with the insertion point and during the surgical instrument insertion stage); Fig. 3b shows the workspace of the parallel robot with the following intervals $\psi = [-60° \; 60°]$, $\theta = [-60° \; 60°]$, $\varphi = [-60° \; 60°]$ to evaluate the parallel robot capability to orient the laparoscope with high angles; Fig. 3c shows the workspace of the parallel robot computed for the commonly used (in SILS [4]) orientations intervals $\psi = [-30° \; 30°]$, $\theta = [-30° \; 30°]$, $\varphi = [-30° \; 30°]$; Fig. 3d shows the parallel robot workspace by considering the insertion point (RCM) R $[X_R = 315.9, Y_R = 701.6, Z_R = 800.6]$ mm, where the center of mobile platform (point E) is a the distance $d = [50\ 100]$ mm from point R (to simulate reorientation and surgical instruments insertion during the SILS task). A trajectory was defined to simulate the SILS task with respect to the insertion point R [$X_R = 315.9$, $Y_R = 701.6$, $Z_R = 800.6$]; the numerical data is shown in Table 2.

Table 2

Numerical data for a SILS trajectory

Stage 1 ($t = [0, 28.4]$ s, $v_{max} = 10$ mm/s, $a_{max} = 5$ mm/s^2)		**Stage 3** ($t = [40.4, 48.5]$ s, $v_{max} = 10$ mm/s, $a_{max} = 5$ mm/s^2)	
Pose 1 [mm, deg] X_E=70.2, Y_E=750, Z_E=860.9, ψ=–45°, θ=0, φ=0.	Pose 2 [mm, deg] X_E=315.9, Y_E=710.6, Z_E=950.5, ψ=0, θ=0, φ=0.	Pose 3 [mm, deg] X_E=315.9, Y_E=701.6, Z_E=850.6, ψ=0, θ=0, φ=0.	Pose 4 [mm, deg] X_E=351.3, Y_E=726.6, Z_E=835.9, ψ=0, θ=45°, φ=–30°
	Stage 2 ($t = [28.4, 40.4]$ s, $v_{max} = 10$ mm/s, $a_{max} = 5$ mm/s^2)		

In **Stage 1** of the trajectory the parallel robot moves from an arbitrary position to an intermediary position where the robot aligns the laparoscope (and the active instruments) with the insertion position (time interval $t = [0, 28.4]$ s).

In **Stage 2** (time interval $t = [28.4, 40.4]$ s) the instruments are inserted in the operating field on a linear trajectory.

In **Stage 3** (time interval $t = [40.4, 48.5]$ s) the parallel robot reorients the medical instruments. The defined trajectory (Fig. 4) was tested in both Matlab and Siemens NX. The trajectory was used as input data for the invers geometric model (computed in Matlab) and the resulted values for the velocities of the active joints (Fig. 5) were exported in Siemens NX (as inputs for the active joints) to simulate the mobile platform motion. Then, the NX data (for the active joints and the mobile platform motion) was exported and plotted in Matlab (Figs. 4 and 5 – black dashed lines) to validate the mathematical model (the Matlab and NX data overlapped with a maximum error of $3 \cdot 10^{-2}$ mm for positioning and 10^{-2} ° for orientations).

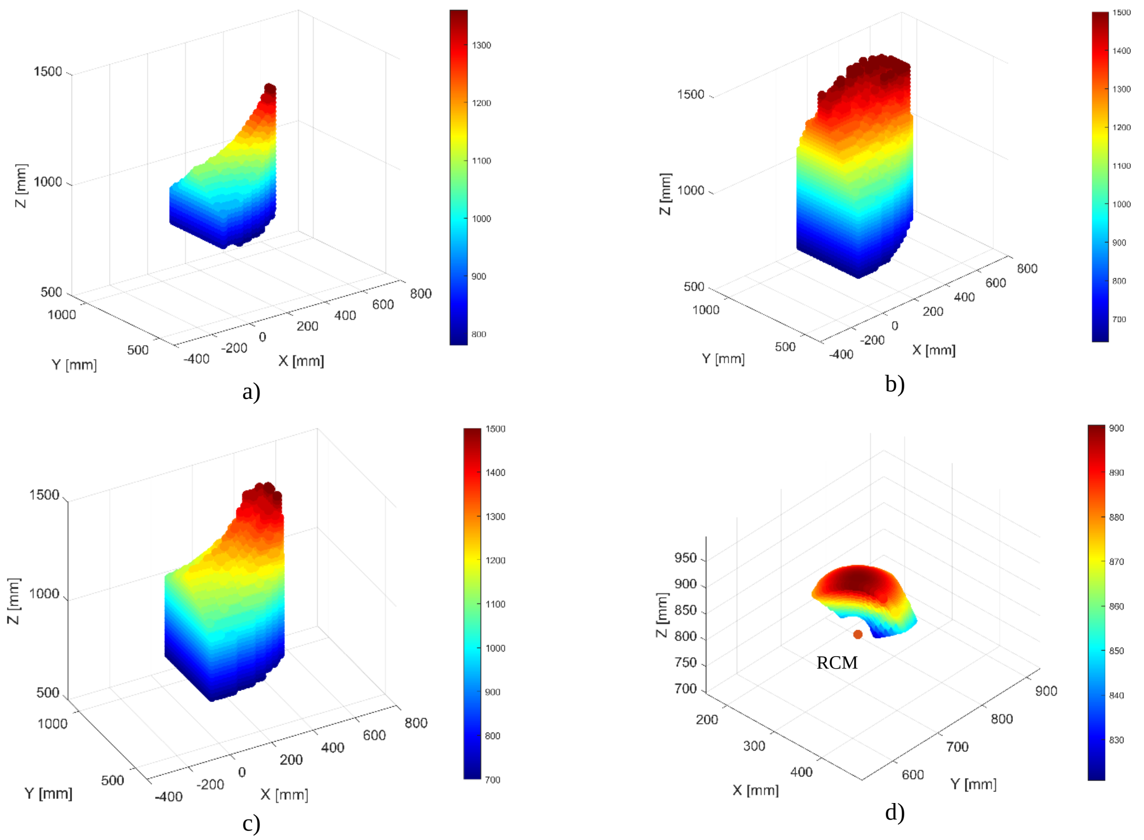

Fig. 3 – Workspace computation for the 6-DOF parallel robot for SILS.

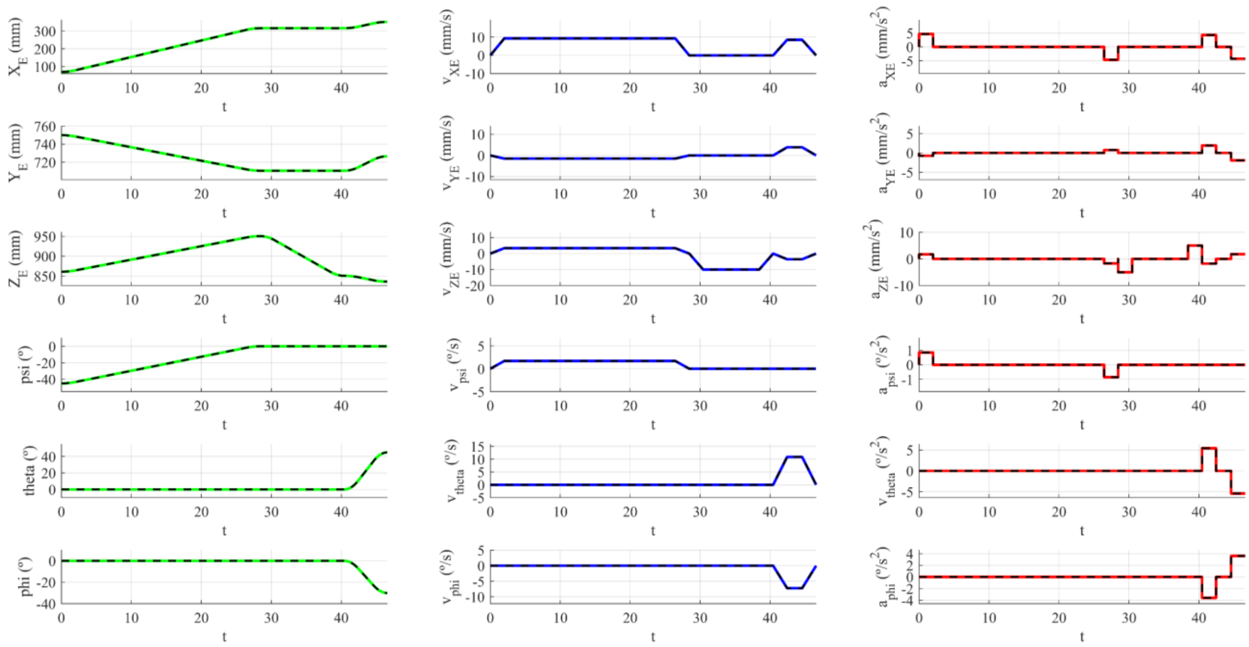

Fig. 4 – Time history diagram for the defined law of motion for the parallel robot mobile platform; green, blue, red lines (Matlab computed data); black dashed lines (Siemens NX exported data).

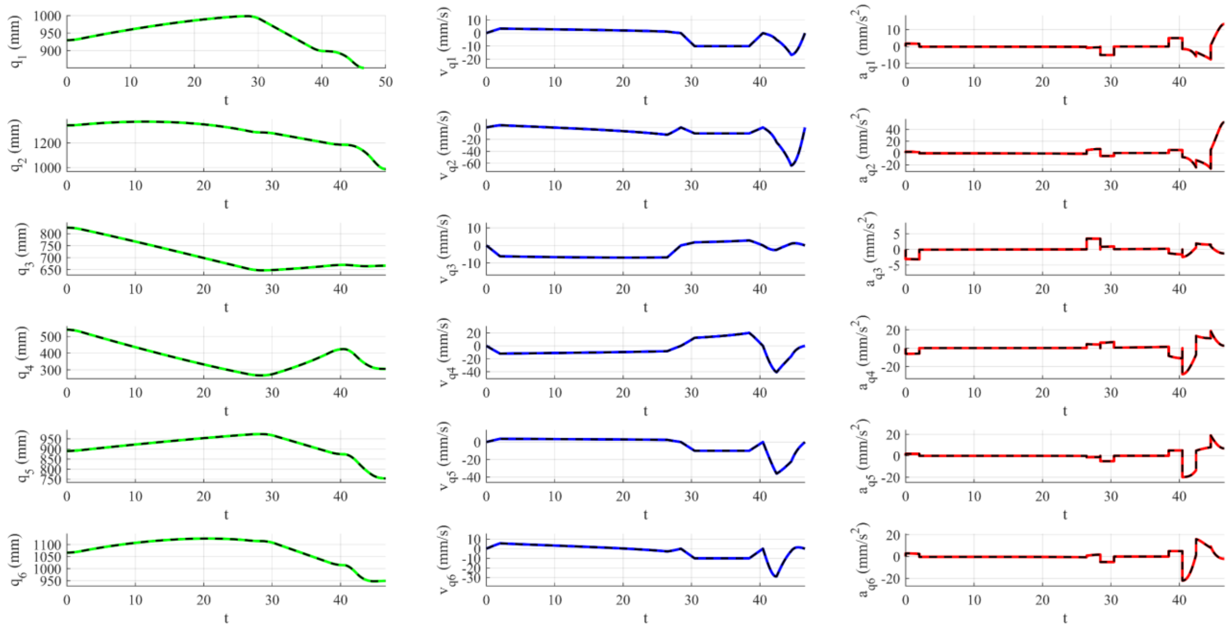

Fig. 5 – Time history diagram for the active joints of the parallel robot; green, blue, red lines (Matlab computed data); black dashed lines (Siemens NX exported data).

5. CONCLUSIONS

The paper presented a 6-DOF parallel robot for SILS with its mathematical modelling and numerical results. The inverse geometric model and the kinematic models were derived using a vector method, achieving fully parametric analytical solutions for the inverse geometric model, whereas the forward geometric model was numerically solved with the NR algorithm. Furthermore, the SILS parallel robot workspace was computed with various constraints, to evaluate the robot capability in different stages of the SILS task. In addition, a SILS trajectory was simulated with respect to a predefined insertion point. The initial numerical results validate the new 6-DOF parallel robot for the SILS medical procedure.

Further work is intended for achieving a complete singularity analysis, corelated with the robot workspace, and dimensional optimization to obtain an optimum workspace and reduce the robot size.

ACKNOWLEDGEMENTS

This work was supported by a grant of the Ministry of Research, Innovation and Digitization, CNCS/CCCDI – UEFISCDI, project number PCE171/2021 – Challenge within PNCDI III, and project POCU/380/6/13/123927–ANTREDOC, "Entrepreneurial competencies and excellence research in doctoral and postdoctoral studies programs", a project co-funded by the European Social Fund through the Human Capital Operational.

REFERENCES

1. W. WANG, X. SUN, F. WEI, *Laparoscopic surgery and robotic surgery for single-incision cholecystectomy: an updated systematic review*, Updates Surg, **73**, *6*, pp. 2039–2046, 2021.
2. M.B. CONNELL, R. SELVAM, S.V. PATEL, *Incidence of incisional hernias following single incision versus traditional laparoscopic surgery: a meta-analysis*, Hernia, **23**, *1*, pp. 91–100, 2019.
3. Y.H. KWAK, H. LEE, K. SEON, Y.J. LEE, Y.J. LEE, S.W. KIM, *Da Vinci SP single-port robotic surgery in gynecologic tumors: Single surgeon's initial experience with 100 cases*, Yonsei Med J, **63**, *2*, pp. 179–186, 2022.
4. D. PISLA, I. ANDRAS, C. VAIDA, N. CRISAN, I. ULINICI, I. BIRLESCU, N. PLITEA, *New approach to hybrid robotic system application in Single Incision Laparoscopic Surgery*, Acta Tehnica Napocensis – Series: Applied Mathematics, Mechanics, and Engineering, **64**, *3*, pp. 369–378, 2021.
5. D. PISLA, D. CARAMI, B. GHERMAN, G. SOLETI, I. ULINICI, C. VAIDA., *A novel control architecture for robotic-assisted single incision laparoscopic surgery,* The Romanian Journal of Technical Sciences – Applied Mechanics, **66**, *2*, pp. 141–162, 2021.
6. W.J. KIM, P.E. PARK, S.B. CHOI, W.B. KIM, *Case report of pure single-port robotic left lateral sectionectomy using the da Vinci SP system, Medicine*., **100**, *51*, art. e28248, 2021.
7. S.D. MCCARUS, *Senhance robotic platform system for gynecological surgery*, JSLS, **25**, *1*, art. e2020.00075, 2021.
8. D. PISLA, B. GHERMAN, N. PLITEA, B. GYURKA, C. VAIDA, L. VLAD, F. GRAUR, C. RADU, M. SUCIU, A. SZILAGHI, A. STOICA, *PARASURG hybrid parallel robot for minimally invasive surgery*, Chirurgia (Bucur), **106**, *5*, pp. 619–25, 2011.
9. D. PISLA, I. BIRLESCU, C. VAIDA, P. TUCAN, B. GHERMAN, N. PLITEA, *Family of modular parallel robots with active translational joints for Single Incision Laparoscopic Surgery* (in Romanian), Patent application OSIM A00733/03.12.2021.
10. X. ZHOU, H. ZHANG, M. FENG, J. ZHAO, Y. FU, *New remote center of motion mechanism for robot-assisted minimally invasive surgery*, BioMed Eng OnLine, **17**, art. 170, 2018.
11. I. BIRLESCU, C. VAIDA, A. PUSCA, G. RUS, D. PISLA, *A new approach to forward kinematics for an orientation platform based on perturbation theory*, 18th International Symposium on Advances in Robot Kinematics, ARK 2022 (eds. O. Altuzarra, A. Kecskeméthy), Proceedings in Advanced Robotics, Vol. 24, Springer, Cham, 2022, pp. 171–178.
12. D. PISLA, N. PLITEA, A. VIDREAN, B. PRODAN, B. GHERMAN, D. LESE, *Kinematics and design of two variants of a reconfigurable parallel robot*, ASME/IFTOMM International Conference on Reconfigurable Mechanisms and Robots, 2009, pp. 624–631.
13. B. GHERMAN, C. VAIDA, D. PISLA, N. PLITEA, B. GYURCA, D. LESE, M. GLOGOVEANU, *Singularities and workspace analysis for a parallel robot for minimally invasive surgery*, IEEE International Conference on Automation, Quality and Testing, Robotics (AQTR), 2010.
14. C. VAIDA, N. CRISAN, I. BIRLESCU, I. ANDRAS, D. PISLA, *Preliminary assessment of artificial intelligence agents for a SILS robotic system*, The 9th IEEE International Conference on E-Health and Bioengineering – EHB 2021, DOI: 10.1109/EHB52898.2021.9657717.
15. M. HUSTY, I. BIRLESCU, P. TUCAN, C. VAIDA, D. PISLA, *An algebraic parameterization approach for parallel robots analysis*, Mechanism and Machine Theory, **140**, pp. 245–257, 2019.

Received March 28, 2022